Radiotracer Dose Reduction in Integrated PET/MR: Implications from National Electrical Manufacturers Association Phantom Studies

Mark Oehmigen[1–3], Susanne Ziegler[1], Bjoern W. Jakoby[4,5], Jens-Christoph Georgi[4], Daniel H. Paulus[1], and Harald H. Quick[1–3]

[1]Institute of Medical Physics, University of Erlangen-Nuremberg, Erlangen, Germany; [2]Erwin L. Hahn Institute for Magnetic Resonance Imaging, University of Duisburg-Essen, Essen, Germany; [3]High Field and Hybrid MR Imaging, University Hospital Essen, Essen, Germany; [4]Siemens Healthcare Sector, Erlangen, Germany; and [5]University of Surrey, Guildford, Surrey, United Kingdom

With the replacement of ionizing CT by MR imaging, integrated PET/MR in selected clinical applications may reduce the overall patient radiation dose when compared with PET/CT. Further potential for radiotracer dose reduction, while maintaining PET image quality (IQ) in integrated PET/MR, may be achieved by increasing the PET acquisition duration to match the longer time needed for MR data acquisition. To systematically verify this hypothesis under controlled conditions, this dose-reduction study was performed using a standardized phantom following the National Electrical Manufacturers Association (NEMA) IQ protocol. **Methods:** All measurements were performed on an integrated PET/MR whole-body hybrid system. The NEMA IQ phantom was filled with water and a total activity of 50.35 MBq of ^{18}F-FDG. The sphere–to–background activity ratio was 8:1. Multiple PET data blocks of 20-min acquisition time were acquired in list-mode format and were started periodically at multiples of the ^{18}F-FDG half-lives. Different sinograms (2, 4, 8, and 16 min in duration) were reconstructed. Attenuation correction of the filled NEMA phantom was performed using a CT-based attenuation map template. The attenuation-corrected PET images were then quantitatively evaluated following the NEMA IQ protocol, investigating contrast recovery, background variability, and signal-to-noise ratio. Image groups with half the activity and twice the acquisition time were evaluated. For better statistics, the experiment was repeated 3 times. **Results:** Contrast recovery, background variability, and signal-to-noise ratio remained almost constant over 3 half-life periods when the decreasing radiotracer activity (100%, 50%, 25%, and 12.5%) was compensated by increasing acquisition time (2, 4, 8, and 16 min). The variation of contrast recovery over 3 half-life periods was small (−6% to +7%), with a mean variation of 2%, compared with the reference setting (100%, 2 min). The signal-to-noise ratio of the hot spheres showed only minor variations over 3 half-life periods (5%). Image readers could not distinguish subjective IQ between the different PET acquisition setups. **Conclusion:** An approach to reduce the injected radiotracer activity in integrated PET/MR imaging, while maintaining PET IQ, was presented and verified under idealized experimental conditions. This experiment may serve as a basis for further clinical PET/MR studies using reduced radiotracer dose as compared with conventional PET/CT studies.

Received Feb. 18, 2014; revision accepted Apr. 21, 2014.

For correspondence or reprints contact: Mark Oehmigen, Erwin L. Hahn Institute for MRI, University of Duisburg-Essen, Arendahls Wiese 199, 45141 Essen, Germany.

E-mail: mark.oehmigen@uni-due.de

Published online Jul. 8, 2014.

Key Words: radiotracer dose reduction; NEMA image quality measurements; integrated PET/MR hybrid imaging; PET/MR phantom measurements

J Nucl Med 2014; 55:1361–1367
DOI: 10.2967/jnumed.114.139147

Integrated PET/MR hybrid imaging in selected clinical applications inherently reduces the overall patient radiation dose when compared with PET/CT by replacing ionizing CT imaging by nonionizing MR imaging. Depending on the clinical indication, replacing CT by MR imaging in the context of PET hybrid imaging theoretically may save half of the overall radiation dose or an even higher fraction when compared with high-resolution diagnostic CT imaging (*1*).

Further potential for radiotracer dose reduction in integrated PET/MR resides in the possibility of decreasing the applied activity deriving from the administered PET radiotracer. PET image quality (IQ) in general is influenced by 2 key factors, acquisition time and injected activity, as both affect count statistics, image signal, and image noise. In PET/MR imaging, radiotracer dose reduction by injecting less tracer activity may be achieved by turning the comparatively prolonged data acquisition times into an advantage. In conventional PET/CT hybrid imaging, the PET data acquisition times typically last around 2–3 min per bed position (*1*). In integrated PET/MR hybrid imaging, MR examinations can be longer and depend on the clinical application. Although data acquisition times in whole-body PET/MR imaging are in the range of 5–10 min per bed position (*2,3*), MR examinations in specific single-bed or single-organ imaging (e.g., head/neck, liver, cardiac, prostate MR imaging) with dedicated multicontrast protocols may last up to 20 min (*4*). These comparatively longer imaging times in PET/MR are associated with acquiring additional diagnostic information based on MR examinations using various contrast weightings and corresponding imaging sequences (Fig. 1). The longer MR examinations, thus, can be considered as the workflow-limiting factor in simultaneous PET/MR imaging. Therefore, adapting and increasing the PET data acquisition times to the prolonged MR examinations may allow for decreasing the injected patient radiotracer activity, compared with clinical PET/CT protocols. Initial results from a clinical study investi-

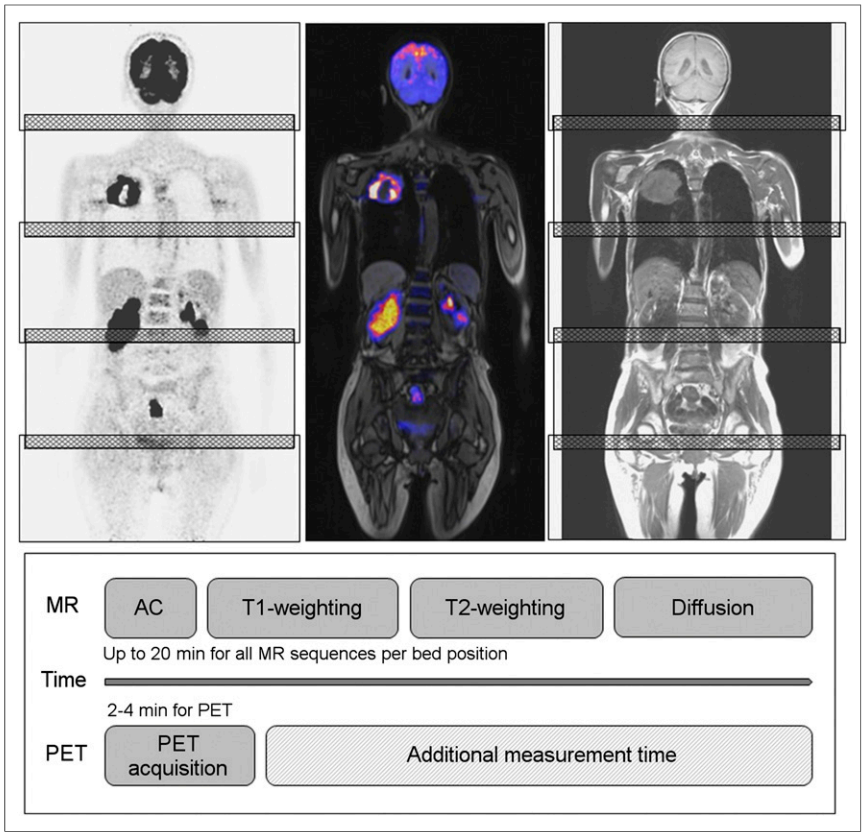

FIGURE 1. Simultaneous PET/MR whole-body data acquisition. PET (left) and MR (right) data acquisitions are performed simultaneously during multistep examination with typically 5 bed positions for whole-body coverage; cross-hatched sections represent overlapping field of view. Standard MR data acquisition encompasses localizer, sequences for AC, and, for example, T1- and T2-weighted imaging for anatomic reference. Further sequences may be added to MR protocol. Simultaneous PET data acquisition requires only 2–4 min per bed position. Relatively longer MR data acquisition times thus provide potential for increased PET data acquisition times.

gating workflow aspects in integrated PET/MR indicated that prolonged PET acquisition times per bed may allow for reduced radiotracer dose (*5*).

To systematically verify this hypothesis under controlled circumstances and to exclude potential biophysical changes in lesion activity over time, the present study was performed using a standardized phantom following the National Electrical Manufacturers Association (NEMA) IQ protocol (*6*). Within this study, 2 aspects of potential radiotracer dose reduction in integrated PET/MR are systematically examined. First, PET IQ is investigated as a function of decreasing radiotracer activity. Second, PET IQ is investigated as a function of decreasing radiotracer activity offset by increasing data acquisition time. IQ in this study has been assessed qualitatively and quantitatively by determination of the following parameters: contrast recovery (CR), background variability (BV), and signal-to-noise ratio (SNR).

MATERIALS AND METHODS

Integrated PET/MR System

All phantom measurements were performed on an integrated PET/MR whole-body hybrid system (Biograph mMR, software version VB20P; Siemens AG Healthcare Sector, Erlangen, Germany), which allows for simultaneous PET and MR imaging (*7*).

The PET detector consists of 8 detector rings of 56 detector blocks each. One detector block is divided into 8 × 8 lutetium oxyorthosilicate scintillator crystal elements read out by 3 × 3 avalanche photodiodes (*8*). The PET detector is fully integrated; therefore, it is positioned between the gradient coil and the radiofrequency body coil of the MR system. The MR system contains an actively shielded 3.0-T superconducting magnet, with a total system length of 199 cm and a patient bore diameter of 60 cm. The gradient coil system provides a maximum amplitude of 45 mT/m and a maximum slew rate of 200 T/m/s.

Phantom Setup

A PET emission phantom was used that is defined by NEMA as a standard for PET IQ determination (Fig. 2) (*6*). The NEMA IQ phantom mimics the shape of an upper human body; it is made of acrylic glass and has an inner volume of approximately 9.5 L. It contains a cylindric inlay filled with a spongeous material with the attenuating properties of human lung tissue. Furthermore, 6 hollow glass spheres with different inner diameters (10, 13, 17, 22, 28, and 37 mm) are located inside the phantom (PTW, Freiburg, Germany). The spheres can be filled with water, with or without the addition of PET radiotracer, to be detected either as hot or cold lesions in contrast to the phantom background volume (Fig. 2).

For the measurements, the 4 smallest spheres were filled with the radioactive PET tracer ^{18}F-FDG, with an activity concentration of 42.4 kBq/mL ± 1% to represent hot

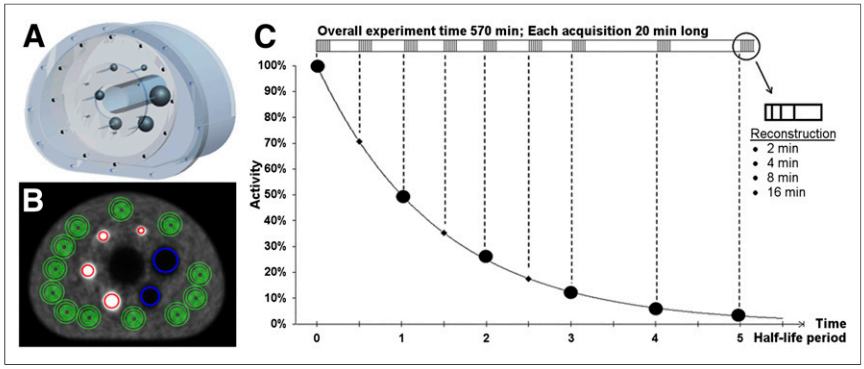

FIGURE 2. (A) Three-dimensional rendering of NEMA IQ phantom. (B) PET image with ROIs marking spheres and background. Four hot lesions and 2 cold lesions are marked with red and blue ROIs, respectively. Altogether, 60 concentric background ROIs (green) are used on each PET image for quantitative evaluation. (C) From beginning of experiment (100% starting activity) and at each subsequent half-life period, list-mode data blocks of 20 min were acquired. Overall, 5 half-life periods (for ^{18}F every 110 min) were covered. In between first 3 half-life periods, additional 20-min data blocks were sampled. Of 20-min list-mode blocks, images were reconstructed with 2-, 4-, 8-, and 16-min acquisition times.

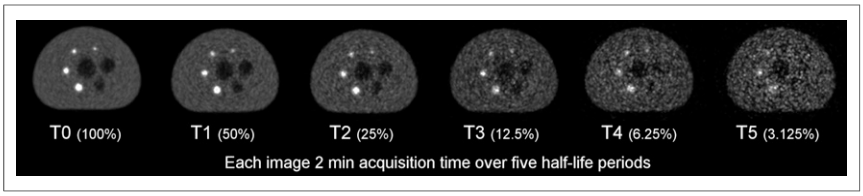

FIGURE 3. PET IQ as function of decreasing radiotracer activity over time. Two-minute data acquisitions were sampled and reconstructed at each of 5 half-life periods. Relative radiotracer activity, compared with starting point (100%), is provided in parentheses.

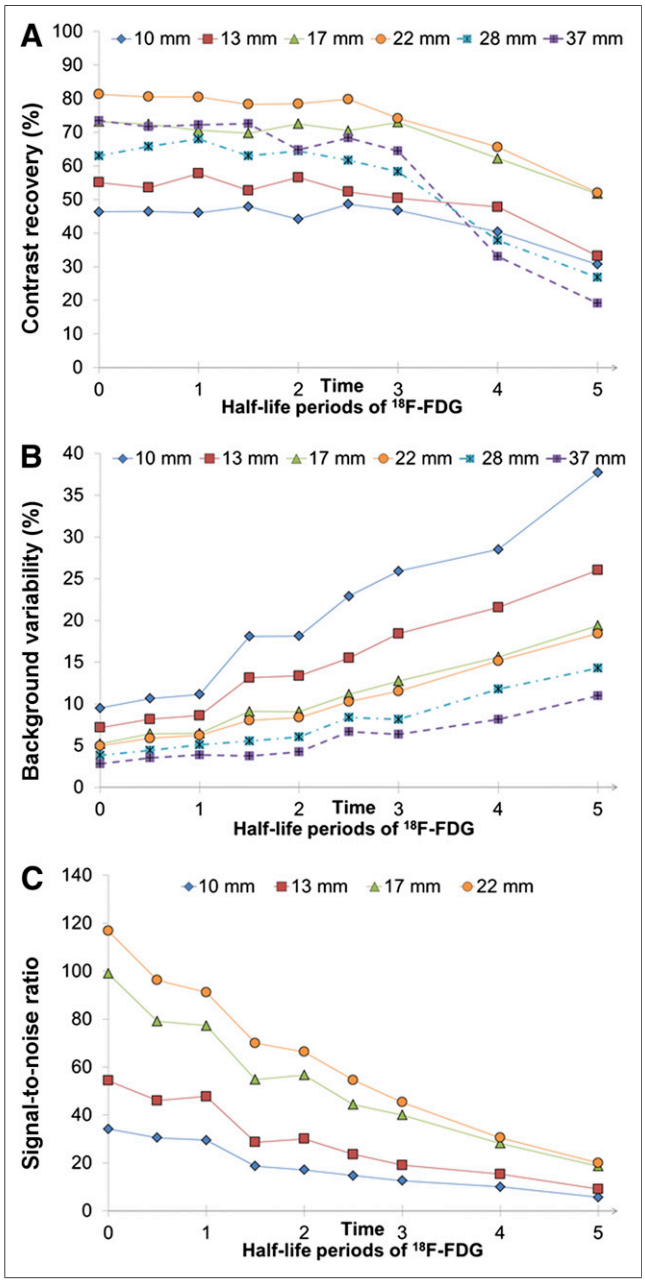

FIGURE 4. Quantitative evaluation of CR (A), BV (B), and SNR (C) as function of decreasing radiotracer activity over time (derived from Fig. 3). Two-minute data acquisitions were sampled and reconstructed at each of 6 half-life periods. (C) SNR was plotted only for 4 hot spheres. All graphs represent mean values from 3 independent experiments. Note that CR for all spheres remains relatively constant up to third half-life period (A).

lesions. The phantom background volume was filled with pure water and 5.3 kBq/mL ± 1% of ^{18}F-FDG, resulting in a sphere–to–background activity concentration ratio of 8:1. The 2 largest spheres were filled with nonradioactive water and therefore represent cold lesions.

To ensure an exact and reproducible position of the phantom in the PET/MR field of view, the phantom was placed on a Styrofoam (The Dow Chemical Co.) holder on the patient table at a predefined table position. This exact placement enables attenuation correction (AC) of the phantom and its fluid fillings with a CT-based template μ map, as described in the following sections.

AC

Human tissue and hardware components, such as phantoms or radiofrequency coils that are placed in the PET field of view during simultaneous PET/MR data acquisition, attenuate PET photons. To obtain quantitative PET images, AC needs to be performed. To correct for attenuation caused by human tissue, MR-based methods for AC are currently applied (*9*), whereas CT-based template μ maps are used to correct for attenuation caused by rigid hardware components such as the patient table and radiofrequency coils (*10,11*). Because it is known that MR-based AC of the NEMA IQ phantom currently considers only the fluid filling but does not account for the phantom housing (*12*), in this study, a CT-based NEMA IQ phantom μ map was generated instead using a 128-slice PET/CT system (Biograph 128; Siemens AG, Healthcare Sector) with the parameters 500 effective mAs and 140 kV. Images were reconstructed with 0.6-mm slice thickness, 512 × 512 image matrix sizes, and a B30f smooth convolution kernel.

The CT-based 3-dimensional phantom template μ map was integrated into the PET/MR system and is defined for a fixed position of the NEMA IQ phantom on the patient table of the PET/MR. Accurate and reproducible positioning of the phantom on the table was achieved using a phantom holder made of Styrofoam, which provides negligible photon attenuation. Because of the exact positioning of the NEMA IQ phantom on the patient table, the location of the phantom matches the CT-based phantom μ map. All PET sinograms were reconstructed using the registered phantom μ map and the hardware μ maps of the PET/MR components (patient table and spine radiofrequency coil) for AC. Qualitative and quantitative image evaluation was thus based on attenuation-corrected PET data.

Imaging Protocol

PET data were acquired as list-mode files to allow for retrospective reconstruction of various measurement durations (2, 4, 8, and 16 min) starting at different points in time. PET list-mode data blocks of 20 min each were recorded. The acquisitions were started periodically at multiples (1–5) of the ^{18}F-FDG half-life (every 110 min) and additionally in between 2 half-lives (Fig. 2C). For improved data statistics, the entire experimental protocol was repeated 3 times in independent measurements.

Experimental Setups for IQ Analysis

IQ as Function of Decreasing Radiotracer Activity. From the multiple acquired 20-min list-mode files, sinograms of specific PET acquisition durations were reconstructed using the e7 reconstruction tools (Siemens AG, Healthcare Sector, Knoxville, TN). To evaluate the impact of the radioactive decay on PET IQ, sinograms of 2-min acquisition duration each were generated at multiples of the ^{18}F-FDG half-life periods. The respective PET images were reconstructed with

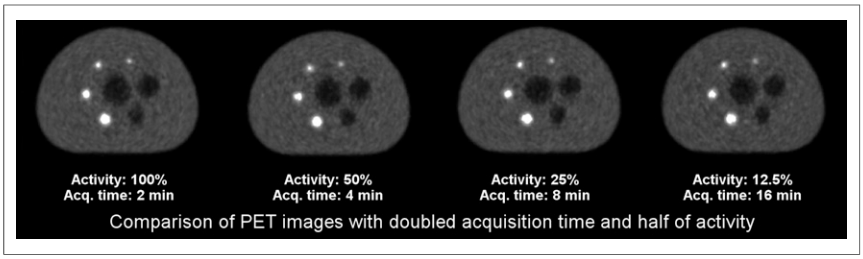

FIGURE 5. PET IQ as function of decreasing radiotracer activity over time while increasing data acquisition times. From left to right, radiotracer activities were divided into half (100%, 50%, 25%, and 12.5% activity) whereas data acquisition times were doubled (2, 4, 8, and 16 min). Differences in resulting overall IQ are hardly perceivable.

a 3-dimensional ordinary Poisson ordered-subsets expectation maximization iterative reconstruction algorithm with the following parameters: 3 iterations, 21 subsets, 344 × 344 image matrix size, 3-dimensional gaussian filter (4 mm). Decay correction was performed for each acquisition block to the start of each phantom experiment (time point T0), which enables the qualitative comparison between the different image datasets. In this experiment, the acquisition time remains 2 min, whereas the activity decreases because of the radioactive decay to 50%, 25%, 12.5%, 6.25%, and 3.125% of the initial 100% activity at time point T0. In addition, 3 intermediate steps between the first half-life periods were recorded.

IQ as Function of Decreasing Radiotracer Activity While Increasing Acquisition Time. In this second set of experiments, data acquisition time was increased while the radiotracer activity inherently reduces over time. More specifically, whereas the tracer activity concentration of the radionuclide ^{18}F was divided into half after every 110 min by radioactive decay, the PET acquisition time was doubled at each half-life period, accordingly. Four datasets were examined and compared, corresponding to activity concentrations and acquisition durations of 100% and 2 min, 50% and 4 min, 25% and 8 min, and 12.5% and 16 min, respectively. The respective PET images were reconstructed with the previously used parameter setting. Similarly, decay correction was performed to the beginning of the phantom experiment.

Quantitative Image Analysis

To analyze and compare all generated PET images quantitatively, the IQ parameters CR and BV, as defined by NEMA, and the SNR were calculated (*6*). For quantitative analysis, the transverse image slice of each dataset was used, in which the maximum diameter of all 6 spheres was depicted. For each sphere, hot or cold, a region of interest (ROI) was drawn to equal diameter as the inner diameter of the respective sphere. In the central slice, additional background ROIs were analyzed. Twelve ROIs with diameters equal to each sphere were investigated in the background of the phantom as shown in Figure 2B. The set of background ROIs are additionally placed in 5 neighboring slices, resulting in 60 background ROIs in total for each sphere size. The analysis was performed with the tool ImageJ (version 1.48a; Wayne Rasband, National Institutes of Health) (*13*).

In these ROIs, the quantitative NEMA image parameters CR and BV were analyzed. The percentage CR for each hot sphere and the corresponding background ROIs is defined by:

$$CR_{Hot} = \left(\frac{\text{ROI hot sphere}}{\text{Mean background}} - 1\right) \Big/ \left(\frac{\text{Activity hot sphere}}{\text{Activity background}} - 1\right),$$

where ROI hot sphere = mean value of an ROI, with specific diameter of a hot sphere; mean background = mean value of all ROIs in the background with the same diameter as the corresponding sphere; activity hot sphere = injected activity in the hot spheres, 42.4 kBq/mL ± 1%; and activity background = injected activity in the background, 5.3 kBq/mL ± 1%.

The percentage CR for each cold sphere was calculated by:

$$CR_{Cold} = \left(1 - \frac{\text{ROI cold sphere}}{\text{Mean background}}\right),$$

where ROI cold sphere = mean value of 1 ROI, with specific diameter as the cold sphere.

The SD was defined by:

$$\text{SD} = \sqrt{\sum_{k=1}^{K=60} (\text{Background value}_k - \text{mean background})^2 \Big/ (K-1)},$$

where $K = 60$, the number of background ROIs in total for each specific sphere size.

The percentage BV for each sphere was calculated by the following equation:

$$\text{BV} = \text{SD} \,/\, \text{mean background}.$$

The third evaluated quantitative parameter is the SNR of the 4 hot spheres, defined as:

$$\text{SNR} = \frac{\text{ROI hot sphere} - \text{mean background}}{\text{Standard deviation}}.$$

Qualitative Image Analysis

In addition to the systematic evaluation of quantitative image parameters, subjective IQ was rated in a masked study. For this purpose, 5 readers who are experienced in the field of hybrid imaging and image processing were instructed to rate and group potential visual differences in IQ. For this evaluation, 16 different images representing a combination of 2-, 4-, 8-, and 16-min acquisitions with 100%, 50%, 25%, and 12.5% activity were reconstructed. Images were presented on a computer using identical window/level settings across all images. The images were then randomized, and the readers were masked to the image acquisition and reconstruction parameters. Readers were asked to group these 16 images from best to worst subjective IQ. In the case of images showing no detectable differences in subjective IQ, readers were asked to sort these images into the same group of comparable IQ.

RESULTS

Quantitative Image Analysis

IQ as Function of Decreasing Radiotracer Activity. The resulting images representing IQ as a function of decreasing radiotracer activity are shown in Figure 3. The measured quantitative IQ parameters CR, BV, and SNR are provided as mean values of 3 independent measurements in Figure 4. The visual degradation of IQ as a function of decreasing radiotracer activity over time is demonstrated (Fig. 3). Image noise increases with decreasing activity concentration over time. The 4 active (hot) and 2 nonactive (cold) spheres are clearly discernible until the activity is reduced to one eighth (12.5%) of the initial activity

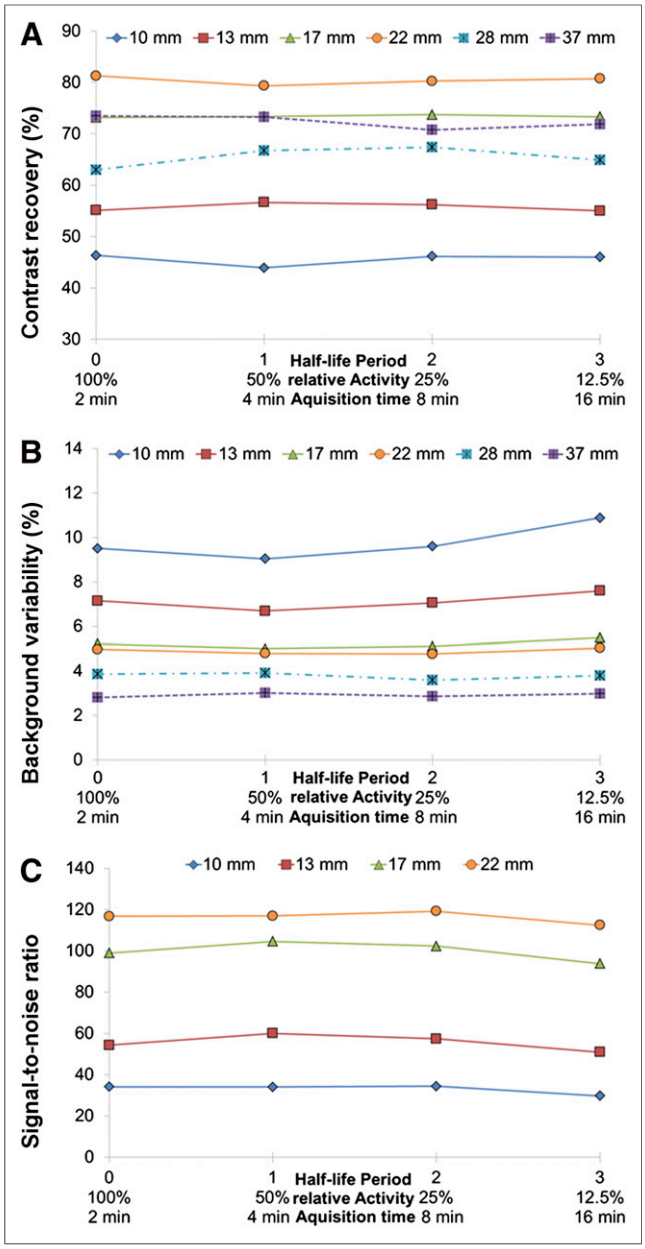

FIGURE 6. Quantitative evaluation of CR (A), BV (B), and SNR (C) as function of decreasing radiotracer activity over time while increasing data acquisition times (derived from Fig. 5). Although radiotracer activities were divided into half (100%, 50%, 25%, and 12.5% activity), data acquisition times were doubled (2, 4, 8, and 16 min). (C) SNR was plotted for only 4 hot spheres. All graphs represent mean values from 3 independent experiments. Increasing acquisition time can compensate reduced radiotracer activity with no notable loss of IQ (consistent CR, BV, and SNR) up to 3 half-life periods.

after 3 tracer half-lives (T3) (Fig. 3). The results of the quantitative evaluation of CR show that CR remains almost constant for up to 3 half-lives (T3) (Fig. 4A). The graphs in Figure 4B and 4C show the increase of BV and a corresponding decrease of SNR for all spheres, respectively.

IQ as Function of Decreasing Radiotracer Activity Offset by Increasing Acquisition Time. The resulting images as a function of decreasing radiotracer activity (100%, 50%, 25%, and 12.5%) and increasing image acquisition times (2, 4, 8, and 16 min) are shown in Figure 5. By visual comparison, no noticeable difference among the 4 images in Figure 5 can be observed. The calculated quantitative IQ parameters CR, BV, and SNR are provided as mean values of 3 independent measurements in Figure 6. Figure 6 shows that CR, BV, and SNR remain almost constant over 3 half-life periods when the decreasing radiotracer activity (100%, 50%, 25%, and 12.5%) is compensated by increasing the data acquisition time (2, 4, 8, and 16 min). The fluctuation of CR over 3 half-life periods is quite small and in the range of −6% to +7%, with a mean variation of 2%, compared with the reference setting (100% activity and 2-min image acquisition time) (Fig. 6A). Only small differences can be observed in the BV. The mean variation of the BV over 3 half-life periods is 4%, with a range from −7% to +13% (Fig. 6B).

The SNR of the 4 hot spheres also shows only minor variations over 3 half-lives (Fig. 6C). The largest variation in SNR was observed for the smallest sphere (diameter, 10 mm), with 15% (at the end of the third half-life) in comparison to the reference image (100% tracer activity and 2-min acquisition time). Otherwise, the SNR remained nearly constant, with a variation of 5% (Fig. 6C). The maximum change in SNR of the 3 larger hot spheres was +10% for the 13-mm sphere, +5% for the 17-mm sphere, and +4% of the 22-mm sphere.

Qualitative Image Analysis

The rating of the subjective IQ by 5 masked and independent reviewers was based on 16 different images that are shown in Figure 7, arranged as a 4 × 4 image matrix. In this figure, all columns are sorted from left to right with decreasing radiotracer activity (100%, 50%, 25%, and 12.5%) and all rows are sorted from top to bottom with increasing image acquisition time (2, 4, 8, and 16 min). For image reading, the images were provided as single images in randomized order, not in a matrix structure. All 5 image readers rated the IQ of the image with 100% activity and 16-min acquisition time as best (Fig. 7, lower left) and the quality of the image with 12.5% activity and 2-min acquisition time as worst (Fig. 7, upper right). All 5 readers grouped the 4 images with 100% and 2 min, 50% and 4 min, 25% and 8 min, and 12.5% and 16 min into the same group 1, indicating comparable subjective IQ (Fig. 7, left upper corner to right lower corner). Three of 5 readers additionally grouped the remaining images into further groups, not showing any subjective IQ differences: group 2 (100% and 8 min grouped with 50% and 16 min), group 3 (100% and 4 min, 50% and 8 min, 25% and 16 min), group 4 (50% and 2 min, 25% and 4 min, 12.5% and 8 min), and group 5 (25% and 2 min, 12.5% and 4 min). The 2 remaining readers each interchanged 1 image only between 2 neighboring groups (group 2 with 3 and group 4 with 5).

DISCUSSION

In this phantom study, the potential for radiotracer dose reduction in integrated PET/MR was explored. The possibility for prolonged PET data acquisition times in PET/MR hybrid imaging provides the basis for reducing radiotracer activity in PET/MR imaging while maintaining high PET IQ. Two effects of reducing radiotracer activity in integrated PET/MR imaging on PET IQ were investigated qualitatively as well as quantitatively using the NEMA IQ phantom. First assessed was the impact of

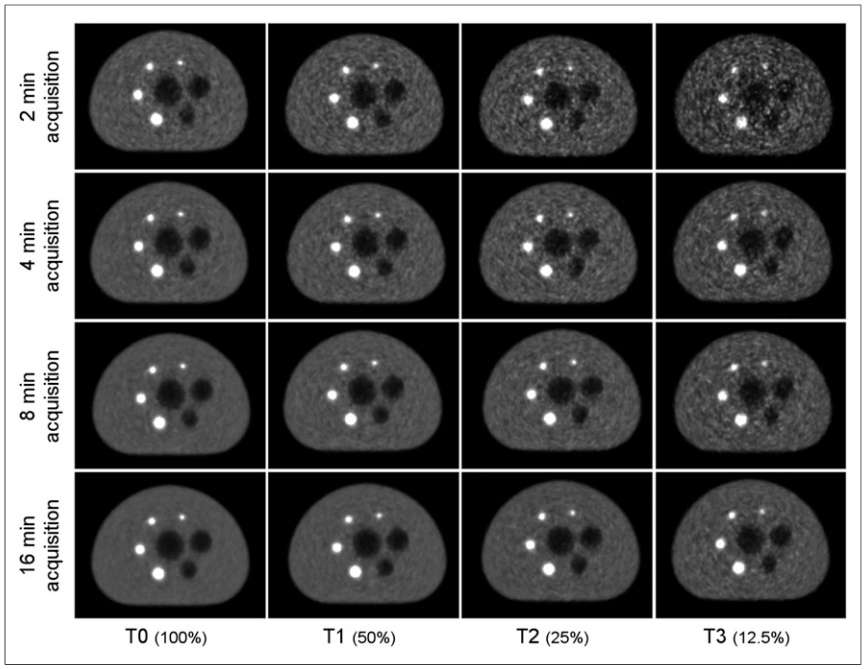

FIGURE 7. Matrix showing IQ as function of decreasing radiotracer activity (left to right column) and increasing acquisition time (top to bottom rows). Diagonal images from top left to bottom right show no perceivable differences in IQ.

reduced radiotracer activity and second the effect of increasing data acquisition times on PET IQ.

To provide a stable and constant hot sphere-to-background ratio activity of 8:1 for each of the spheres over the course of each experiment, the study was set up so that the NEMA IQ phantom was injected with radiotracer only once. Measurements with decreasing radiotracer activity were obtained by repeated measurements over multiple half-life times of the radionuclide ^{18}F rather than by reinjecting progressively lower activities into individual spheres and into the background volume. Additionally, the potential impact of different data acquisition times on the results was minimized by list-mode PET data acquisition over 20 min and subsequent reconstructions of 2-, 4-, 8-, and 16-min acquisition blocks. The 3-fold repetition of the whole experimental setup and subsequent data evaluation provided improved statistics and the evaluation of mean values and variation. The evaluation of the IQ beyond the course of four ^{18}F half-lives, while further increasing the PET measurement times, was not evaluated in this study, to remain within clinically applicable measurement constraints.

When the impact of reduced tracer activity was investigated, the qualitative and quantitative results demonstrated that all spheres (hot and cold) are visible up to 3 half-life periods when the initial tracer activity has decayed to only 12.5% of the initial value. Down to this reduced tracer activity, the CR for all spheres remains largely stable whereas the BV increases and the SNR decreases with reduced tracer activity, as expected.

Assessing the effect of increasing data acquisition times qualitatively and quantitatively demonstrated that increasing the data acquisition time can compensate for reduced tracer activity while maintaining PET IQ and lesion detectability up to a factor of 8 (i.e., 12.5% of the initial tracer activity and 16-min acquisition time instead of 2 min).

Although all qualitative and quantitative results of our study indicate high IQ and sphere-to-background detectability up to an 8-fold-reduction of tracer activity, it needs to be considered that this phantom study was performed under controlled circumstances. Before conclusions for a clinical application of tracer activity reduction can be drawn, further factors such as biodistribution of the tracer in different lesions and background over time, as well as associated tracer washin and washout phenomena, need to be considered that ultimately may influence lesion detectability in vivo (*1,14*). The results of this study, however, confirm the general potential for application of reduced radiotracer activity in the context of integrated PET/MR hybrid imaging. A reduction in radiotracer activity by one half seems realistic when transferring the results of this phantom study to a clinical setting.

Prolonging PET data acquisition times in general may potentially lead to increased influence of patient motion, such as breathing, cardiac motion, and overall motion of the patient on IQ and lesion detection. Because of the nature of a phantom study, the impact of motion on IQ has not been investigated in this study. On the other hand, the simultaneous MR acquisition may provide the means to detect and correct for patient motion in a clinical setting.

CONCLUSION

The hypothesis to maintain PET IQ at lower injected tracer activity by increasing the acquisition time is viable, as shown in this phantom study and under idealized experimental conditions. In this study, an approach to taking advantage of the prolonged PET/MR patient examinations is proposed that may lead to reduced radioactive tracer dose. This reduction of tracer dose can be accomplished by increasing the PET acquisition duration to match the amount of time needed for the MR patient examination. The results of this study demonstrate the validity of the proposed hypothesis and identify a further advantage of integrated PET/MR hybrid imaging in the context of reducing patient radiation exposure.

DISCLOSURE

The costs of publication of this article were defrayed in part by the payment of page charges. Therefore, and solely to indicate this fact, this article is hereby marked "advertisement" in accordance with 18 USC section 1734. This work was supported by, and the Biograph mMR PET/MR system at the Institute of Medical Physics (University of Erlangen-Nuremberg) was funded through a research collaboration between, Siemens Healthcare Sector, Erlangen, Germany, and the University of Erlangen-Nuremberg. No other potential conflict of interest relevant to this article was reported.

ACKNOWLEDGMENTS

We thank Jens U. Krause, Institute of Medical Physics, University of Erlangen-Nuremberg, for PET tracer handling during all NEMA phantom measurements.

REFERENCES

1. Boellaard R, O'Doherty MJ, Weber WA, et al. FDG PET and PET/CT: EANM procedure guidelines for tumor PET imaging—version 1.0. *Eur J Nucl Med Mol Imaging.* 2010;37:181–200.
2. Drzezga A, Souvatzoglou M, Eiber M, et al. First clinical experience with integrated whole-body PET/MR: comparison to PET/CT in patients with oncologic diagnoses. *J Nucl Med.* 2012;53:845–855.
3. Quick HH, von Gall C, Zeilinger M, et al. Integrated whole-body PET/MR hybrid imaging: clinical experience. *Invest Radiol.* 2013;48:280–289.
4. Martinez-Möller A, Eiber M, Nekolla SG, et al. Workflow and scan protocol considerations for integrated whole-body PET/MRI in oncology. *J Nucl Med.* 2012;53:1415–1426.
5. Hartung-Knemeyer V, Beiderwellen KJ, Buchbender C, et al. Optimizing positron emission tomography image acquisition protocols in integrated positron emission tomography/magnetic resonance imaging. *Invest Radiol.* 2013;48: 290–294.
6. National Electrical Manufacturers Association. NEMA standards publication NU 2-2007. *Performance Measurements of Positron Emission Tomographs.* Rosslyn, VA: NEMA; 2007:26–33.
7. Delso G, Fürst S, Jakoby B, et al. Performance measurements of the Siemens mMR integrated whole-body PET/MR scanner. *J Nucl Med.* 2011;52:1914–1922.
8. Pichler BJ, Judenhofer MS, Catana C, et al. Performance test of an LSO-APD detector in a 7-T MRI scanner for simultaneous PET/MRI. *J Nucl Med.* 2006;47: 639–647.
9. Martinez-Möller A, Souvatzoglou M, Delso G, et al. Tissue classification as a potential approach for attenuation correction in whole-body PET/MRI: evaluation with PET/CT data. *J Nucl Med.* 2009;50:520–526.
10. Delso G, Martinez-Möller A, Bundschuh RA, et al. Evaluation of the attenuation properties of MR equipment for its use in a whole-body PET/MR scanner. *Phys Med Biol.* 2010;55:4361–4374.
11. Paulus DH, Tellmann L, Quick HH. Towards improved hardware component attenuation correction in PET/MR hybrid imaging. *Phys Med Biol.* 2013;58: 8021–8040.
12. Ziegler S, Braun H, Ritt P, et al. Systematic evaluation of phantom fluids for simultaneous PET/MR hybrid imaging. *J Nucl Med.* 2013;54:1464–1471.
13. Schneider CA, Rasband WS, Eliceiri KW. NIH Image to ImageJ: 25 years of image analysis. *Nat Methods.* 2012;9:671–675.
14. Zhuang H, Pourdehnad M, Lambright ES, et al. Dual time point ^{18}F-FDG PET imaging for differentiating malignant from inflammatory processes. *J Nucl Med.* 2001;42:1412–1417.